EFDA–JET–PR(06)23

E. Minardi, C. Sozzi, P. Mantica and JET EFDA contributors

Stationary Magnetic Entropy Tokamak States and Experimental Observations

Stationary Magnetic Entropy Tokamak States and Experimental Observations

E. Minardi, C. Sozzi, P. Mantica and JET-EFDA contributors*

[1]*Istituto di Fisica del Plasma del CNR,EUR-ENEA-CNR Association Via R. Cozzi, 53 20125 Milano Italy*
** See annex of M.L. Watkins et al, "Overview of JET Results ", (Proc. 21st IAEA Fusion Energy Conference, Chengdu, China (2006)).*

Preprint of Paper to be submitted for publication in
Nuclear Fusion

ABSTRACT.

The assumption that the tokamak magnetic configuration at equilibrium is associated with the stationary magnetic entropy and with minimum plasma thermal energy leads to the prediction of definite profiles for the induced current density and for the pressure. These profiles should characterize the states spontaneously assumed by the tokamak under normal conditions (to be defined in the text).

The theoretical results are compared with the observations collected from different tokamaks, plasma regimes and heating methods, taking into account the possible existence of non inductive currents. The comparison allows the identification of the limits of validity of the model and confirms the robustness, within these limits, of the magnetic entropy concept for the description of the "privileged" tokamak states.

1. INTRODUCTION

The equilibrium of the plasma confined in a magnetic field is completely determined when the distribution of the current density and of the pressure is known together with the external physical and geometrical conditions. However the current density and the pressure are not fully fixed by the equation describing the static magnetic equilibrium (e.g. the Grad-Shafranov equation) in view of the arbitrary functions involved by this equation. Surely the macroscopic equilibrium is the result of the complex dynamics of the underlying system of particles subject to individual as well as to collective interactions. Notwithstanding this complication, one could ask whether these interactions may result finally in a spontaneous selection among the infinite possibilities allowed by the arbitrariness of the equation, a selection operated innerly by the plasma itself when it is not forced artificially toward a specific configuration by external interventions. According to this point of view one is led naturally to consider that to the equilibrium states of the plasma could correspond suitably defined probabilities whose relative measure determines the selection among all possible states of the fluctuating system. That is, one could introduce the possibility space of all current density distributions (conveniently coarse-grained) and define the probability p_i of each distribution (labeled by i) under suitable constraints. We have adopted the point of view of information theory where the constraints have a hypothetical meaning to be confirmed by the experimental test. The collective (macroscopic) equilibrium state of the plasma is introduced through the constraints and is characterized in the statistical model by the fact that it is independent of the effects at the individual particle level, as is the case of collective systems described by Vlasov equation [1]. The entropy defined by the classical relation of information theory $S = -\sum_i p_i \ln(p_i)$ will then provide the interpretative tool for inserting the state selection based on probability in the framework of a generalized thermodynamics.

Following this line of thought one arrives at the concept of "magnetic entropy" [1], a functional of the macroscopic current density $\vec{j}$ and of the vector potential $\vec{A}$, whose variation properties determine the "privileged" plasma equilibria:

$$S\{\vec{j},\vec{A}\} \propto -\int j^2 dV + \frac{\mu^2 c}{4\pi}\int \vec{j}\cdot\vec{A}dV \qquad (1.1)$$

where μ is a parameter (a Lagrange multiplier) whose role will be illustrated in the text.

The present paper is dedicated to the comparison with the experiment of the privileged states predicted by the variation properties of (1.1) in the case of a stationary tokamak. The tokamak is an open system in interaction with the external world through the Ohmic transformer and the auxiliary power. Since the system is not isolated, the entropy is not required to be maximum, but it can be assumed to be stationary *even locally*, expressing the local balance between the entropy injected externally and the entropy produced in the plasma. This assumption leads to an equation for the inductive current density [1,2] whose aspects in cylindrical circular geometry will be discussed in section 2. In section 3 we discuss the thermodynamic relation that holds under stationary conditions between this equation and the electron transport in the domain of validity of the theory. In section 4 we present the form of the pressure profiles derived, according to refs.[2,3], from the requirement that the total plasma thermal energy is stationary (in general minimum) for fixed magnetic entropy (1.1) and for fixed plasma *induced* current. One obtains a one-parameter family of suitably normalized pressure profiles, each profile (in general concave) being fixed by the value of the total thermal energy of the plasma.

In section 5 the theoretical results for the current density and for the pressure are compared with the observations in a number of discharges in different tokamaks, with different plasma regimes and heating methods (see Table I). The domain of validity of the theory is clearly illustrated considering situations with strong non inductive currents or when the current profile is artificially modified by external interventions (e.g. for generating an internal transport barrier). Finally, section 6 contains the conclusion and the Appendix gives information about the correction that is applied for taking into account the noncircular geometry.

2. STATIONARY MAGNETIC ENTROPY (SME) AND THE EQUATION FOR THE CURRENT DENSITY

The SME equation for the current density in a tokamak, whose predictions will be compared with the observations, has the form [1]

$$\frac{\vec{E}}{\mu^2}\cdot\nabla j + \vec{E}\cdot\vec{j} + p_E = 0 \qquad (2.1)$$

where $\vec{E} = E\vec{e_\phi}$ is the externally induced electric field. We shall discuss later in this section the role, connected with the loop voltage, of the parameter μ. In section 3 it will be shown, on the ground of the consistency of eq.(2.1) with the electron power balance, that the quantity p_E is the net power density (auxiliary power minus non diffusive losses) deposited on electrons in addition to the term $\vec{E}\cdot\vec{j}$, under the thermodynamic conditions consistent with the stationary entropy.

The current density in eq.(2.1) is the inductive current driven by the electric field $\vec{E}$. In general the total current density will be the sum of inductive and non inductive parts (neglecting a possible interaction between the two parts)

$$\vec{j}_{tot}(r) = \vec{j}(r) + \vec{j}_{nind}(r) \tag{2.2}$$

The form of $\vec{j}_{nind}(r)$ depends on the specific mechanism that creates it (the mechanism of bootstrap and that of the current drive by electromagnetic fields or neutral injection) and it is taken from experiment, that is, it is calculated from their generation mechanism consistently with the experimental data. Eq.(2.1) is expected to hold when the plasma settles in an asymptotical relaxed situation in the absence of a strong non inductive drive and outside the region where macroscopic dynamical processes (e.g. sawteeth) are present. In general the zone of relaxation is a bounded region, the so called "confinement region". This excludes the central region of the discharge dominated by sawteeth up to the value $q(r_1) \approx 1$ of the safety factor and the edge region with $r > sa$ where s is a fraction of the minor radius a and sa corresponds to some value of r outside the surface with $q = 2$.

Eq.(2.1) is solved in cylindrical circular geometry. A correction for noncircular geometry is applied to the calculation of integral quantities like the total current, the poloidal magnetic field and the safety factor (see Appendix).

The boundary value of $j(r)$ at $r = sa$ is taken from experiment as well as the loop voltage U and the electric field $E = U/2\pi R$. The value at the inner boundary $r = r_1$ depends on the physical situation in the central region $r < r$ and will be discussed in section 5. The parameter μ is then used to fit the solution to the given boundary conditions and the given U. This is achieved in general for a value of μsa lower than one (see Table II). The profiles become rather insensitive to changes of μsa (and of U) below this value. Also they are rather insensitive to the intensity and the detailed form of the power deposition p_E (profile consistency). Indeed p_E enters eq.(2.1) through the term $\mu^2 pE / E$ which tends to be essentially invariant with respect to changes of the factors [3], while $p_E(r)$ determines the current density profile through a double integration (see eq.(4.3)) which smoothes out the detailed form of the power deposition.

When the relaxed region reaches the minor axis (e.g. in the case $q(0) > 1$ the solution is fixed by requiring the vanishing of the derivative of $j(r)$ at $r = 0$ and the value of $j(r)$ at $r = sa$. However in the cases considered here the relaxation region of the current does no include the axis and the solution is obtained by taking from the experiment the values of the current density at the inner and outer boundaries of this region.

3. THERMODYNAMIC RELATION BETWEEN THE SME EQUATION AND THE ELECTRON THERMAL TRANSPORT

Let us compare the integral of the SME equation (2.1) with the power balance of the electrons

carrying the induced current

$$-\int_{V_p} \frac{\vec{E}}{\mu^2} \cdot \nabla^2 \vec{j} dV = \int_{V_p} \vec{j} \cdot \vec{E} dV + \int_{V_p} p_E \, dV$$
$$-\int_{S} \vec{q}_h \cdot d\vec{S} = \int_{V_p} \vec{j} \cdot \vec{E} dV + \int_{V_p} p_E \, dV \qquad (3.1)$$

where $\vec{q}_h$ is the thermal flux of the electrons and S is the surface enclosing the plasma volume V_p. It follows that in the SME states the thermal flux is related to the derivative of the current density

$$\int_S \vec{q}_h \cdot d\vec{S} = -\int_{V_p} \frac{\vec{E}}{\mu^2} \cdot \nabla^2 \vec{j} dV = -\frac{1}{\mu^2} \int_S (E \nabla j - j \nabla E) \cdot d\vec{S} \qquad (3.2)$$

provided that p_E is the net non Ohmic power density deposited on electrons. In this way the stationary entropy condition expressed by the first equation (3.1) implies the power balance expressed by the second equation (3.1).

Assuming for simplicity cylindrical circular geometry, one can easily express the heat flux across the outer surface $S = 4\pi^2 rR$ in terms of the ratio $s_h(r)/q(r)$ between the magnetic shear s_h and the safety factor. Indeed combining the relation

$$j(r) = \frac{c}{4\pi t} \frac{d}{dr} (rB_\theta) = \frac{cB}{4\pi Rr} \frac{d}{dr} \left(\frac{r^2}{R(r)} \right) \qquad (3.3)$$

with the expression (3.2) one obtains

$$q_h S = \frac{cBU}{\mu^2 R} \left(\frac{s_h}{q} + \frac{1}{2} \frac{d}{dr} \left(\frac{s_h}{q} \right) + const \right) \qquad (3.4)$$

where the constant is fixed by the boundary condition at the inner border of the confinement region. The heat flux is then expressed in terms of the magnetic configuration, which in turn depends on the power deposited on electrons **t**hrough the SME equation. In order to determine the temperature one needs a constitutive relation, for instance

$$-n_e \chi_{eff} \frac{dT_e}{dr} = q_h \qquad (3.5)$$

The electron temperature T_e, calculated from eq.(3.5), is therefore the result of the combined effect of the magnetic configuration at hand and of the thermal transport described by the specific form of χ_{eff}.

4. PRESSURE PROFILE OF THE SME STATES

The pressure profile will be expressed in terms of the poloidal flux ψ, which is determined in the cylindrical limit by the D'Alembert equation

$$\nabla^2\psi = \frac{4\pi R}{c}\, j_{tot} \tag{4.1}$$

where $\psi = -RA_\phi$ (A_ϕ is the axial component of the vector potential). One has a simple relation between ψ and the solution j of eq.(2.1). Taking into account (2.2) and (4.1), eq.(2.1) becomes

$$\nabla^2\left(j + \frac{c\mu^2}{4\pi R}\,\psi\right) = -\frac{\mu^2}{E}(p_E - Ej_{nind}) \tag{4.2}$$

After a double integration one obtains

$$j = -\frac{c\mu^2\psi}{4\pi R} - (\mu sa)^2 \int_0^x \frac{dx}{x} \int_0^x \pi_E(x)\, x dx + D_0 1g\, x + D_1 \tag{4.3}$$

Here $x = r/sa$ where sa is the outer border of the integration zone (the confinement zone), D_0 and D_1 are integration constants to be fixed by the boundary conditions on the current density and

$$\pi_E(x) = \frac{p_E(x) - Ej_{nind}(x)}{E} \tag{4.5}$$

The pressure profile is determined applying the variation procedure previously introduced in refs. [2,3], namely we assume that the plasma thermal energy in the confinement zone

$$W = \frac{3}{2}\int p(\psi)\, dV \tag{4.6}$$

is stationary (it turns out to be minimum in the practical cases) with respect to variations $\delta\psi$ such that the total *induced* current $I_{ind} = \int 2\pi jrdr$ and the magnetic entropy (defined by (1.1) with the *induced* current density (4.3)) are fixed

$$\delta(W + \eta_1 S + \eta_2 I_{ind}) = 0 \tag{4.7}$$

where $\delta j = -(\mu^2/4\pi R)\delta\psi$ (consistently with (4.3)) and η_1 and η_2 are Lagrange multipliers. This requirement leads to the following equation for the pressure [2,3]

$$\frac{dp}{d\psi} = \eta_1 \left(\frac{c\mu^4(sa)^2}{6\pi R}\int_1^x \frac{dx}{x}\int_0^x \pi_E(x)\, x dx - \frac{c\mu^2 D_0}{6\pi R}\, 1g(x) - \frac{c\mu^2 D_1}{6\pi R}\right) + \eta_2\, \frac{c\mu^2}{12\pi^2 R^2} \tag{4.8}$$

The integration of this equation gives $p(x)$ once $\psi(x)$ is known ($\psi(x)$ is calculated from (4.1) after solving (2.1) for j). There are three constants to be determined, namely η_1, η_2 and the integration constant of (4.8) (the constants D_0 and D_1 are fixed by the boundary conditions on the current density, see next section). The values of p at the two boundaries of the integration zone (to be taken from the experiment) leave us with one constant free. This constant can be expressed in terms of the

plasma thermal energy in the integration zone (this is related to the width and to the concavity of the pressure profile). We refer for the details to [2,3]. We are then restricted by the variation procedure above to a one-parameter family of pressure profiles. In order to fix a specific profile of the family one should solve the equations of transport. Here we take from the experiment the value of the total plasma thermal energy of the discharge at hand.

The treatment above holds in the large aspect ratio limit of the toroidal equilibrium described by the Grad-Shafranov equation. For the treatment of the SME model in toroidal geometry see refs.[2,3]. The consistency of the SME equation (2.1) and of the principle of minimum plasma energy with the Grad-Shafranov equation imposes strong constraints on the arbitrary functions entering into this equation. This leads naturally to the calculation of the effect of poloidal currents on the toroidal field. Here the toroidal field is assumed as purely external and uniform.

5. SME STATES AND EXPERIMENTAL OBSERVATIONS

The first step of the analysis consists in a standard interpretative transport simulation performed with a transport code (JETTO, ASTRA, CRONOS, EVITA), using for the input profiles the experimental data, including, for part of the JET shots, the safety factor calculated taking into account the Motional Stark Effect. This process produces the radial profile of the inductive current density and of the pressure to be compared with that predicted by the SME equations (2.1) and (4.8).

The natural field of application of the SME model concerns relaxed states in which the dissipation processes are counterbalanced by external sources (Ohmic or auxiliary) such that the magnetic entropy and the plasma state are constant in time. On the basis of the data collected from different machines [4], we are able to analyze with our method different heating scenarios, from highly localized EC heated plasmas of FTU and TS to broader electron heating obtained in JET using the Mode Conversion ICRF. The effects of high magnetic field (7.2T) and high electron density are studied in a set of Ohmic shots of FTU. The results on quasi- circular plasmas of FTU and TS can be compared with those on the elongated plasma of JET. Different confinement regimes are explored as well, comparing L-modes of FTU, TS, and JET with H-mode, ITB and Hybrid Mode cases of JET.

Table I shows the characteristic parameters of the discharges analyzed in this paper (for the definition of the geometrical parameters k_{e0} and k_{e1} see the appendix). We concentrated mainly on auxiliarly heated discharges, as the case of purely Ohmic discharges has been already studied in TCV [2,5]. The SME equations are solved in a relaxed zone $sa\lambda \le r \le sa$ using for E the experimental value obtained from the loop voltage and taking from experiment the values of j and p at the boundaries. The input p_E to (2.1), which gives the net non Ohmic power on electrons, is supplied by the interpretative transport codes. Table II shows the parameters involved in the solution of (2.1) and (4.8) and the quantities

$$erj = \sqrt{\frac{\sum_i (j_{SME}(r_i) - j_{exp}(r_i))^2}{\sum_i (j_{exp}(r_i))^2}}, \qquad erp = \sqrt{\frac{\sum_i (p_{SME}(r_i) - p_{exp}(r_i))^2}{\sum_i (p_{exp}(r_i))^2}}, \tag{5.1}$$

which are a measure of the adherence of the theoretical current density and pressure profiles to the experimental ones in the region $sa\lambda \le r \le sa$. The loop voltage *U(V)* is not critical for the determination of the profiles because a change of U can be compensated to some extent by a change of μ as is clear by inspecting equation (2.1). The value of s gives the upper limit of the confinement region and a good fit is generally obtained for $0.75 < s < 0.95$ with a mean square deviation (5.1) lower (often much lower, see Table II) than 10%.

In the discussion of the data of the Tables we distinguish two cases depending whether the safety factor q_0 on axis is lower or larger than one.

5.1. SHOTS WITH $q_0 < 1$*:*

In the presence of sawteeth the inner boundary $sa\lambda$ should fixed in the neighborhood of the surface $q = 1$. It is instructive to check the sensitivity of the results to the choice of the inner boundary surface. In fig.1 the mean square deviation is calculated from (5.1) with the theoretical current density normalized at the experimental value on the inner boundary surface $q = 1$ and with the experimental current density normalized to its value at a displaced surface $q = 1 + \Delta q$. The mean square deviation is plotted as function of the position of this surface, labeled by Δq, and one sees that it remains significantly below 10%, and practically insensitive to q for $q > 1$. At the contrary, in many cases, the deviation increases rapidly when q decreases below one, denoting a worsening of the adherence between the theoretical and the experimental current density profiles in the region dominated by the sawteeth.

It is worthwhile to point out a difference in the dependence of the current density on the poloidal flux in the L and H discharges, which fact could be useful for the understanding of the L-H transition. As shown by some examples in fig.2 the *j(ψ)* curve (where the *entire* dependence of $\vec{j}$ on $\vec{r}$ is expressed through $\psi(r)$) is concave in the case of the L shots (fig.2a) and is linear in the case of the H shots (fig.2b) up to $r \approx 0.85a$. It has been shown [1] that the linear dependence of j on ψ is associated with a state of absolute maximum of the magnetic entropy. Therefore one should expect that the plasma is evolving spontaneously towards this state from the L-state provided that the transition is sufficiently rapid for considering the system as isolated from the external world during the transition time. From the thermodynamic point of view the situation is the same as that of the states described by the Taylor's model of the reversed field pinch. The force free states correspond as well to the absolute maximum of the entropy [1] with $\vec{j} \sim \vec{A}$ ($\vec{A}$, vector potential). Consequently they should be reached spontaneously in a pinch configuration provided that the plasma could be considered as isolated from the external world (e.g. enclosed in a perfectly conductive shell and not

subject to auxiliary heating). This condition is verified only approximately in practical devices.

In the following figures typical situations extracted from the list of Table I are illustrated in detail by plotting the experimental and theoretical current density and pressure profiles, as well as the experimental non Ohmic net power deposition p_E on electrons, which is a mark of the discharge. In figs. 3 to 9 the value of q on the minor axis is lower than one, while in figs.10 to 11 it is larger. In the former case the theoretical profiles are calculated in the region $q \geq 1$. The experimental profiles were measured at a time (specified in the plots) when the discharge can be considered as stationary. In fig.3 we present an example of the ECRH discharge in FTU (shot 18290). In this shot the EC power (0.85MW) is deposited in a single location (in shot FTU 18281, also listed in the Tables, the same EC power is distributed in two different locations) For further details on these shots see ref.[3]. Figs.4 and 5 present examples of Ohmic and EC discharges in TS (shots 31165oh and 31165ec respectively), while fig.6 (JET 44013) gives an example of the NBI heated H-state, where the geometrical effects of the elongation have been taken into account in the theoretical calculations (see Appendix).

Figures 7 and 8 are examples of JET L-discharges in which the total current density profile includes non inductive currents (bootstrap+current due to NBI) (shots 55805 and 55809).

Figure 9 is an example (JET 50630) of a H-discharge with significant non inductive current (0.22MA) in a high density plasma ($n_{e0} = 0.71 \cdot 10^{20}$ m^{-3}).

Shots with $q_0 > 1$**:** In order to compare the theory with not relaxed situations and to gain a comprehensive view of its limits of validity, we have considered a variety of current density profiles. The list of table I includes cases where the current profile has been controlled at the centre by external interventions such as ramps-up and non inductive current drive in order to modify the q profile and generate an internal transport barrier (shots JET 53298, 58148, 59397, 59211, 53506). As we shall see, the region of validity of the SME profiles is restricted to those values of λ_{sa} which exclude the region where strong external modification of the current has taken place.

Figure 10 gives an example (JET 53298) of a current density with a small hole on axis (figure 7(b) circles) associated with a value of the safety factor larger than one ($q_{min} \approx 1.3$). Figure 7(b) (line) shows the solution of the SME equation with derivative vanishing on axis and with the boundary value at $sa = 0.75m$ taken from the experiment. The solution disagrees with the experiment in the central region but agreement, both for the current density and particularly for the pressure, is recovered when the SME equations are solved outside this region, taking the experimental values at the borders (figs.7(c) and 7(d).

Figure 11 presents the interesting case with an intense non inductive current (bootstrap+current due to NBI) near the central axis (JET 58148, $q_{min} \approx 1.5$). Figure 11(a) shows the additional net power deposition on electrons and fig.11(b) shows the plot of the total experimental (circles) and theoretical (line) current density as well as the non inductive part (dots). The theoretical curve is the sum of the non inductive part and the induced part obtained by solving the SME equation (2.1) assuming a derivative vanishing on the minor axis and taking the experimental value for the inductive current

density at the border $sa = 0.90m$. One sees from fig. 11(b) that the theoretical profile disagrees strongly in the central region, as expected, but it rejoins the experimental profile outside the region of large non inductive current. We then solve the SME equation in this region i.e. $0.36 < r(m) < 0.90$, taking the experimental values of j and p at the inner and outer borders. With this additional information the theoretical and experimental profiles of the current density and of the pressure agree in the region above, as shown in the figs.11(c) and 11(d).

The same situation occurs in the case of the discharge 59397 with the net electron power deposition shown in fig.12(a). In this case a deep central hole in the current profile is created by the combined effects of the ramp-up of the current, of the bootstrap current and of the Lower Hybrid-NBI+ICRH heating, in order to generate an internal transport barrier. Figure 12(b) shows how the theoretical profile, which deviates strongly in the centre from the experimental one, rejoins the experimental behavior outside the region where the central hole was artificially created. Figures 12(c) and 12(d) show the satisfactory adherence of the theoretical and experimental profiles in the outside region $0.42 < r(m) < 0.95$ where the SME equations are solved.

The other shots with $q_{min} > 1$ listed in Table II are treated with the same procedure as above: first one solves the SME equation in the whole interval from $r = 0$ to $r = sa$ in order to determine the region of adherence between theory and experiment. Then the SME equation is solved again in this region with the appropriate boundary conditions.

Recently two papers appeared [6], [7], in which the experimental indications on the profile consistency, collected from different machines, are discussed. In ref.[7] the experiments are compared with the assumption that the "canonical" current density and pressure profiles are proportional, i.e. $j \sim p$. It is also stated that "in the SME theory an unambiguous connection between canonical current and pressure profiles is not established". In fact the relation $j \sim p$ *assumed* in ref.[7], has been *derived* from the SME model in the Ohmic case (see ref.[8], eqs.(14) and (16)). In the presence of auxiliary heating the simple relation above is not valid and the profiles of j and p are described by the more flexible SME equations (2.1) and (4.8). The insensitivity of the SME equilibrium to the intensity and the form of the deposited power profile is contained in the properties of invariance of these equations.

CONCLUSIONS

In the absence of strong external artificial interventions such as intense non inductive drive, the current density and pressure profiles assumed spontaneously by the plasma at equilibrium in the tokamak can be derived from general variation principles. These principles follow from an extension of the thermodynamic formalism to high temperature (collisionless) magnetic plasma equilibria, based on probability and information [1], which leads to the magnetic entropy functional (1.1). The induced current density is described by eq. (2.1), which is derived from the condition that the magnetic entropy of the tokamak, considered as an open system, is stationary locally (the SME condition). The pressure profile is described by eq.(4.8), which follows from SME, combined with the requirement that the plasma thermal energy is minimum.

Within its limits of validity, the description based on the equations above is of surprising precision and simplicity. These results are of theoretical as well of practical interest. They are of theoretical interest because they establish the reliability of the thermodynamic point of view, which allows, under certain conditions, the description of the plasma equilibrium without resorting to the complicated mathematics of the dynamical treatment for eliminating the arbitrariness implicit in the Grad-Shafranov equation. They are of practical interest because they imply that the transport coefficients are so constrained as to adapt the transport to the equilibrium determined by the general variation principles. The global point of view offered by thermodynamics, though independent of the detailed dynamical mechanisms, allows the unraveling of those phenomenological parameters, which are at the heart of the physical process and which are therefore worthy of the more specific dynamical analysis. One example is the observation on the H-states indicated in fig.2, which points to a specific thermodynamic distinction between the L- and H-states, worthy of a more detailed inspection susceptible of fruitful results. Thus, once the soundness of the variation principles is established, one can proceed to analysing the experimental data on transport in the light of the new point of view.

The electron temperature is described by the transport equation (3.5) in which the right hand side can be expressed in terms of the magnetic configuration, while the left hand side contains the transport effects embodied by the thermal electron diffusivity. Through this equation the electron transport adapts flexibly to the magnetic equilibrium imposed by the variation properties of the magnetic entropy and of the plasma energy.

Last but not least, the extension of the functional (1.1) to the case of electric charge or mass distributions and the associated potentials, opens new perspectives for the treatment of the macroscopic collisionless electrostatic and self-gravitating equilibria.

APPENDIX:

CORRECTION FOR A CYLINDRICAL GEOMETRY WITH ELONGATION

A geometrical correction for noncircular geometry, even though approximate, is applied to the calculation of all integral quantities (total current, total power, magnetic poloidal flux and so on) by expressing the volume element with the cylindrical coordinates $x = r\cos\theta, y = rk_e(r)\sin\theta$, where the elongation is given by the expression $k_e(r) = (k_{e1} - k_{e0})/r/a + k_{e0}$. One obtains (after averaging over the angle).

$$dxdy = 2\pi J(r)rdr \text{ with } J(r) = k_e(r) + (r/2)dk_e/dr \qquad \text{(A1)}$$

One then defines an effective current density $j_{eff}(r) = j_{tot}(r)J(r)$, and an effective poloidal magnetic field given by the equation

$$\frac{1}{r}\frac{d}{dr}(rB_\theta) = \frac{4\pi}{c}j_{eff}(r) \qquad \text{(A2)}$$

The safety factor is obtained from the expression

$$q\,(r) = \frac{cr^2 B_\phi}{2RI(r)} \frac{1 + k_e^2(r)}{2} \qquad \text{(A3)}$$

where $I(r) = 2\pi \int_0^r j_{eff}(r)\, rdr$.

The expression (4.8) for the pressure is also corrected by introducing the Jacobian $J(x)$ in the integral involving the power density (the effective power being $p_E(x)J(x)$) and expressing the poloidal flux ψ with the effective magnetic field given by (A2).

Clearly the correction above holds only for a large aspect ratio and is defective when toroidal geometrical effects become important.

ACKNOWLEDGEMENTS

The authors are indebted to Sandro Jacchia and Enzo Lazzaro for useful suggestions and comments**.** The authors are also indebted to B. Esposito, F. Imbeaux, M.Marinucci and M. Romanelli for their contribution to the collection of the data.

REFERENCES

[1]. Minardi, E. 2005 J. Plasma Phys. **71** 53

[2]. Minardi, E. and Weisen, H. 2001 Nucl. Fusion **41** 113

[3]. Minardi, E., Lazzaro, E., Sozzi, C. and Cirant, C. 2003 Nucl. Fusion **43** 369

[4]. Sozzi et al. Proc. 20th Int. Conf. on Fusion Energy 2004 (Vilamoura, Portugal, 2004) (Vienna:IAEA) paper TH/P6-13 http://www-naweb.iaea.org/napc/physics/fec/fec2004/datasets/index.html

[5]. Weisen, H. and Minardi, E. 2001 Europhys. Lett. **56** 542

[6]. Razumova, K.,A., Andreev V., F., Donne' A., et al. 2006 Plasma Phys. Control. Fusion **48** 1373

[7]. Dnestrovskij, Yu., N., Razumova, K., A., Donne' et al. 2006 Nucl. Fusion **46** 953

[8]. Minardi, E. 1998 Phys. Lett. **A 240** 70.

TABLE I

MacR/a	**Shot**	**Regime**	**Main Heating**	**I(MA)**	**$n_{e0}10^{-20}$**	**B_0(T)**	**k_{e0}**	**k_{e1}**	**P_α(MW)**
FTU0.97/0.30	18290	L	ECRH	0.40	1.13	5.70	1.03	1.02	0.85
FTU	18281	L	ECRH	0.40	1.28	5.80	1.03	1.02	0.85
FTU	23053	L	OHMIC	1.10	1.35	7.20	1.03	1.02	0.0
FTU	23179	L	OHMIC	1.40	2.60	7.20	1.03	1.02	0.0
TS2.42/0.75	31165oh	L	OHMIC	1.00	0.30	3.865	1.0	1.05	0.0
TS	31165ec	L	ECRH	1.00	0.30	3.85	1.0	1.05	0.80
JET3/1	44013	H	NBI	2.60	0.68	2.70	1.40	1.75	15
JET	55805	L	NBI +ICRH	1.60	0.23	3.36	1.25	1.60	6.1
JET	55809	L	NBI +ICRH	1.60	0.26	3.25	1.30	1.60	12
JET	53298	H	NBI	2.20	0.56	2.60	1.35	1.73	15
JET	50630	H	NBI +ICRH	2.80	0.71	2.76	1.40	1.70	12.5
JET	58148	H	NBI +ICRH	1.80	0.29	3.40	1.40	1.75	18
JET	59397	ITB	NBI +ICRH	2.80	0.33	3.45	1.63	1.75	17
JET	56083	H	NBI +ICRH	2.50	1.15	2.70	1.34	1.85	15
JET	62789	Hyb	NBI +ICRH	2.60	0.32	3.20	1.30	1.63	20
JET	59211	H	NBI	1.80	0.53	2.80	1.25	1.50	12
JET	53506	e-ITB	NBI +ICRH	2.40	0.16	3.40	1.35	1.63	6.0
JET	53822	L	ICRH	1.90	0.35	3.40	1.30	1.60	6.0
JET	55802	L	NBI +ICRH	1.60	0.29	3.25	1.27	1.60	6.0
JET	53299	H	NBI	2.50	0.12	2.70	1.35	1.73	15.5
JET	50628	H	NBI +ICRH+	2.80	0.60	2.77	1.37	1.70	12.6

TABLE II

Mac	**Shot**	μsa	**U(V)**	**s**	λ	Δq	**erj**	**erp**
FTU	18290	0.20	1.0	0.73	0.17	1-3.94	0.042	0.022
FTU	18281	0.03	1.0	0.75	0.15	1-3.93	0.071	0.035
FTU	23053	0.15	1.73	0.80	0.55	1-2.15	0.086	0.023
FTU	23179	0.03	2.60	0.80	0.62	1-1.72	0.033	0.034
TS	31165oh	0.01	0.80	0.93	0.20	1-4.13	0.068	0.011
TS	31165ec	0.10	0.55	0.93	0.22	1-4.09	0.070	0.043
JET	44013	0.30	0.20	0.75	0.44	1-2.15	0.031	0.027
JET	55805	0.05	0.33	0.90	0.12	1-5.88	0.039	0.086
JET	55809	0.01	0.40	0.75	0.13	1-3.92	0.076	0.063
JET	53298	0.30	0.15	0.75	0.26	1.41-3.22	0.042	0.022
JET	50630	1.70	0.35	0.90	0.16	1.03-2.78	0.079	0.040
JET	58148	0.10	0.20	0.90	0.40	2.17-5.36	0.035	0.040
JET	59397	0.65	0.60	0.95	0.44	1.71-4.33	0.042	0.026
JET	56083	0.25	0.25	0.80	0.51	1-2.11	0.022	0.036
JET	62789	0.25	0.70	0.70	0.35	1.02-2.60	0.075	0.036
JET	59211	0.10	0.20	0.80	0.19	1.25-3.93	0.026	0.024
JET	53506	0.10	0.20	0.90	0.44	1.76-4.20	0.043	0.043
JET	53822	0.05	0.40	0.70	0.23	1-3.48	0.077	0.039
JET	55802	0.40	0.30	0.75	0.15	1-3.55	0.030	0.060
JET	53299	0.05	0.20	0.80	0.45	1-2.21	0.042	0.044
JET	50628	0.10	0.35	0.95	0.20	1.03-3.24	0.115	0.025

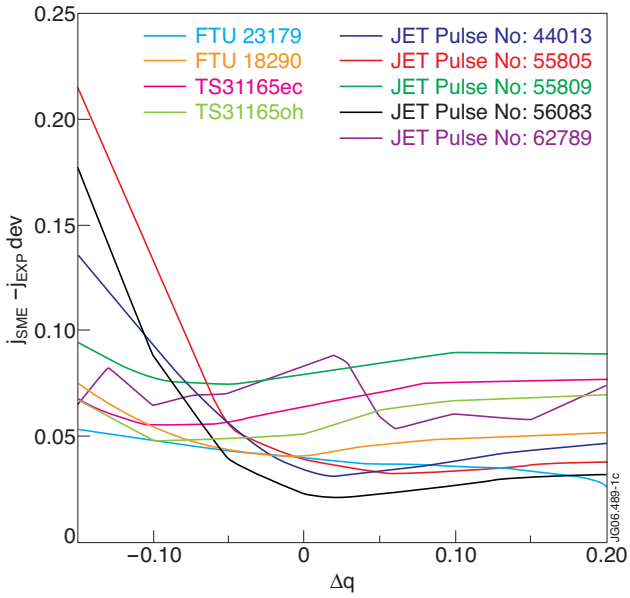

Figure 1: The mean square deviation of the theoretical current density profile with respect to the experimental profile when j_{SME} and j_{EXP} are normalized on inner boundary surfaces displaced by Δq.

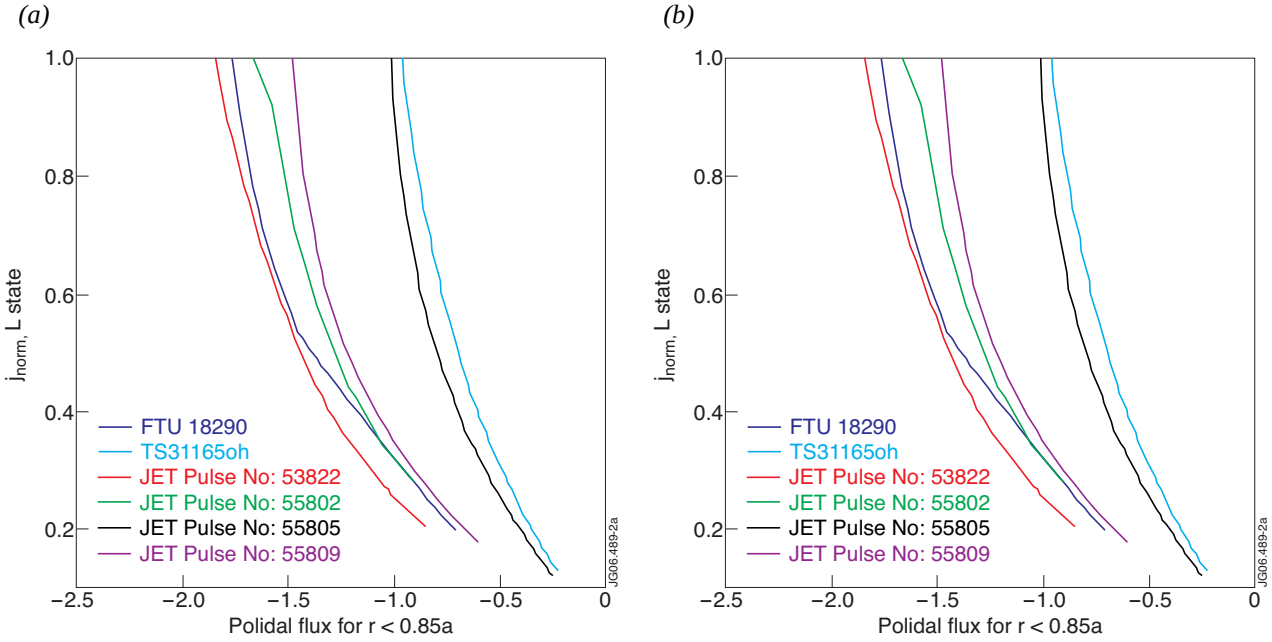

Figure 2: Dependence of the normalized current density on $\Psi = \psi / (sa)^2$ (where ψ is the poloidal flux in Tesla $\cdot$ m^2 divided by 2π) in the range from q = 1 to r = 0.85a, according to experimental equilibrium reconstruction: (a) L-states; (b) H-states.

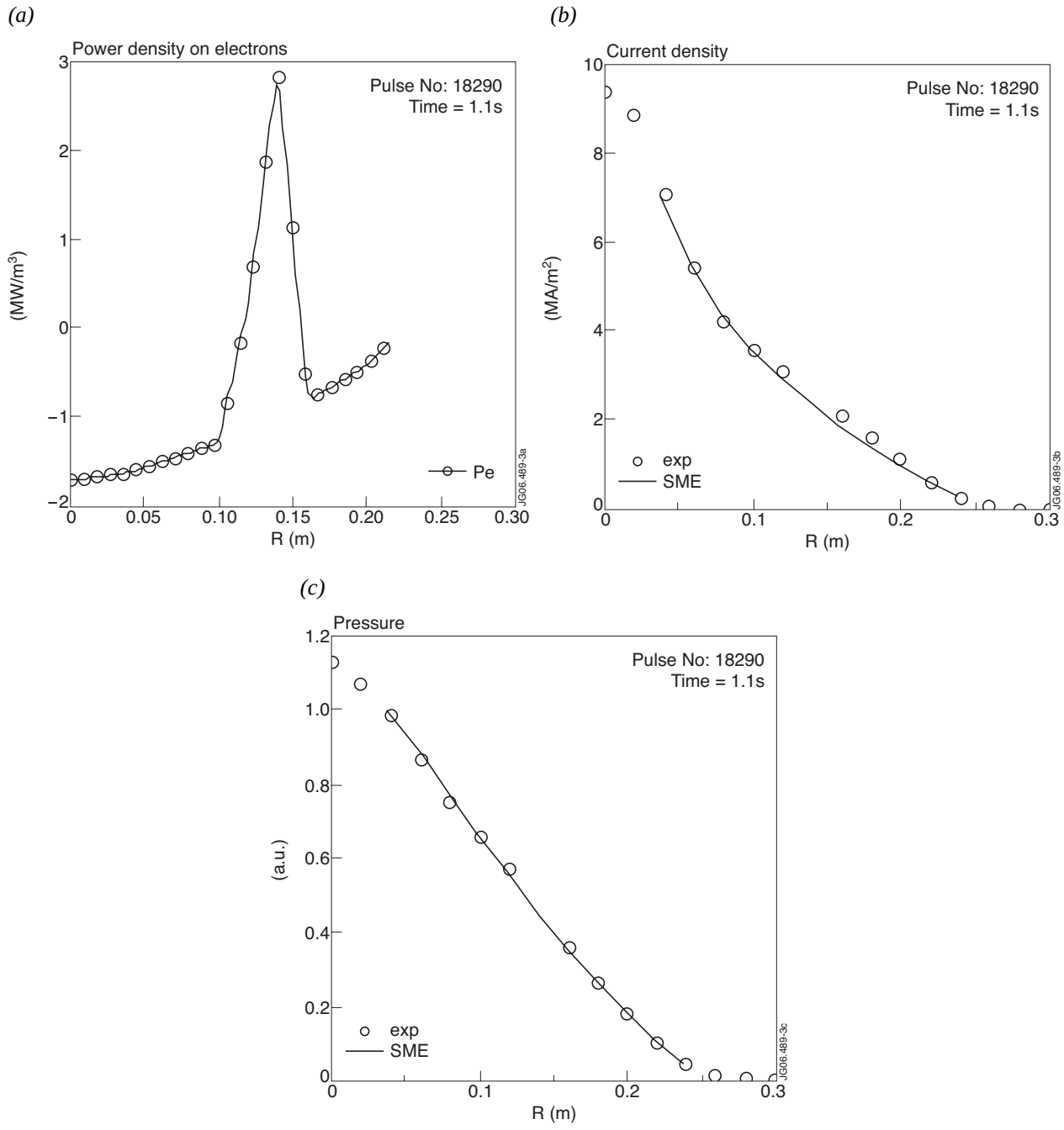

Figure 3: FTU 18290 with EC heating; (a) radial profile of the non Ohmic power density on electrons; (b) theoretical (line) and experimental (circles) profiles of the current density in the range 1<q<3.94 of the safety factor; (c) theoretical (line) and experimental (circles) pressure profiles in the same range, normalized on the surface q=1.

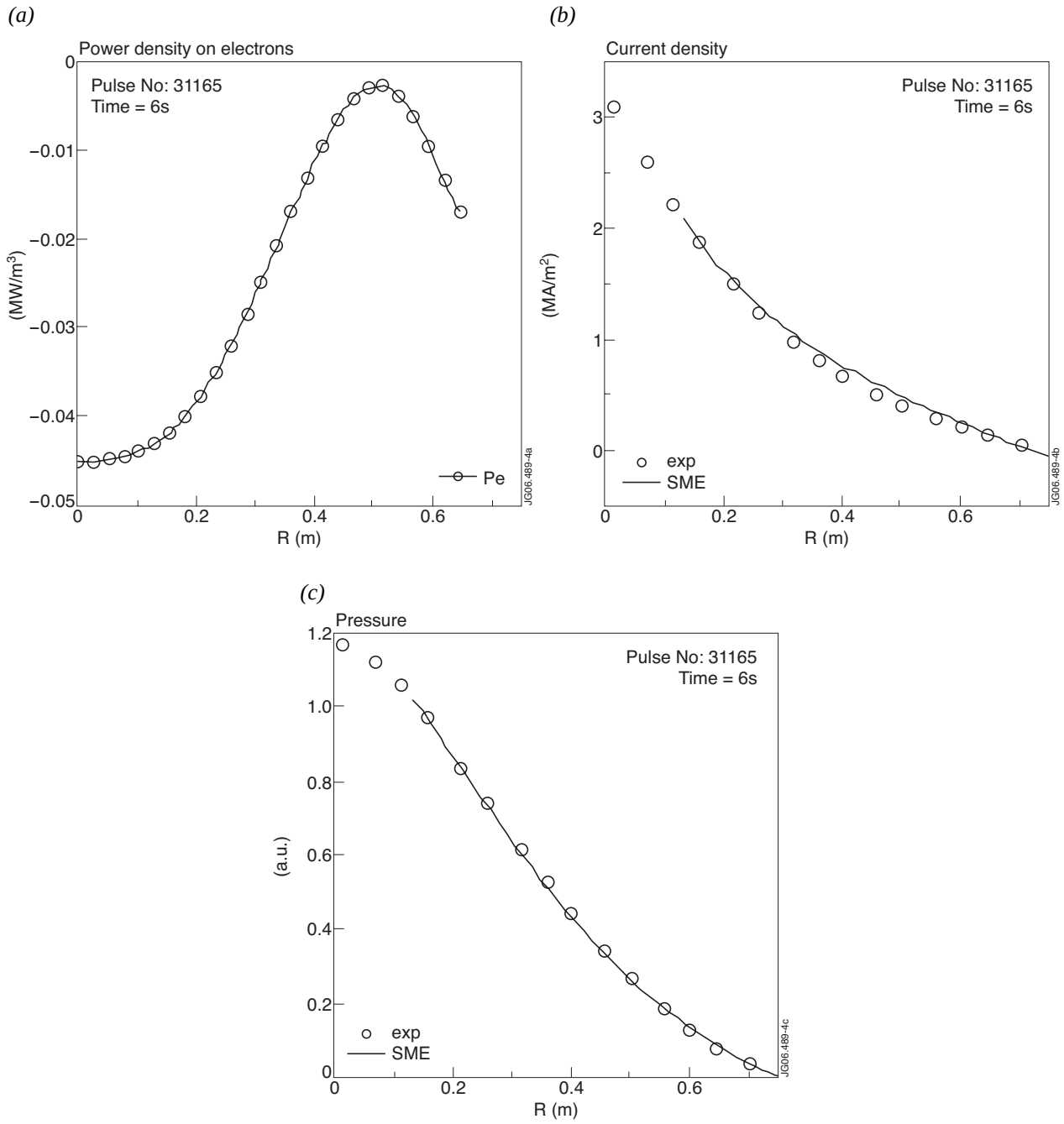

Figure 4: TS 31165oh; (a) radial profile of the non Ohmic power density on electrons; (b) theoretical (line) and experimental (circles) current density profiles in the range 1<q<4.13 (including 0.14MA of non inductive current) and (c) the corresponding normalized pressure in the same range.

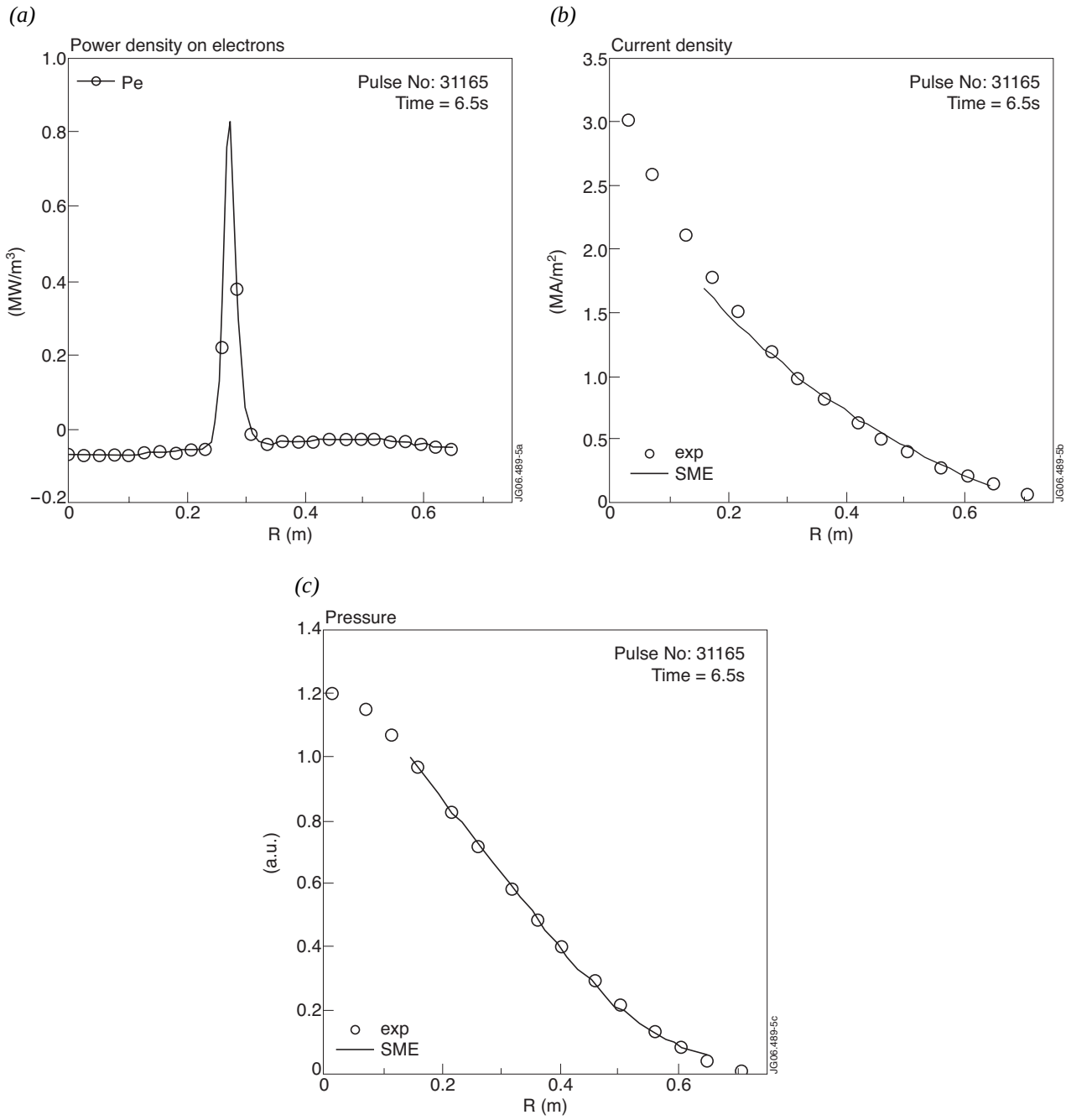

Figure 5: TS 31165ec with EC heating; (a) radial profile of the non Ohmic power density; radial theoretical (line) and experimental (circles) profiles of the current density (b) (including 0.14MA of non inductive current) and of the normalized pressure (c) in the range 1<q<4.09.

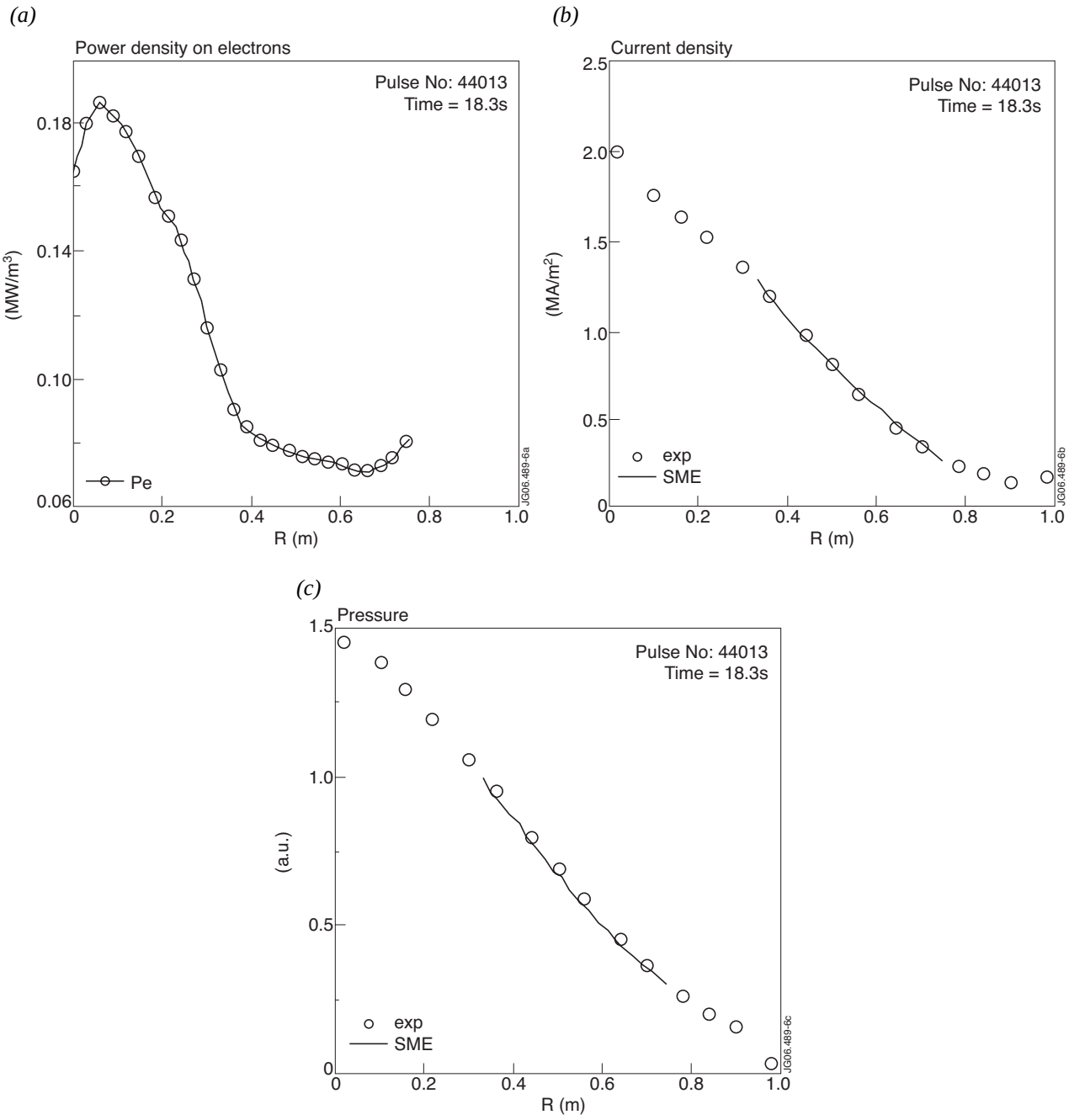

Figure 6: JET Pulse No: 44013 NBI heated H state; (a) radial profile of the non Ohmic power density on electrons; radial theoretical (line) and experimental (circles) profiles of the current density (b) and of the normalized pressure (c) in the range 1<q<2.15.

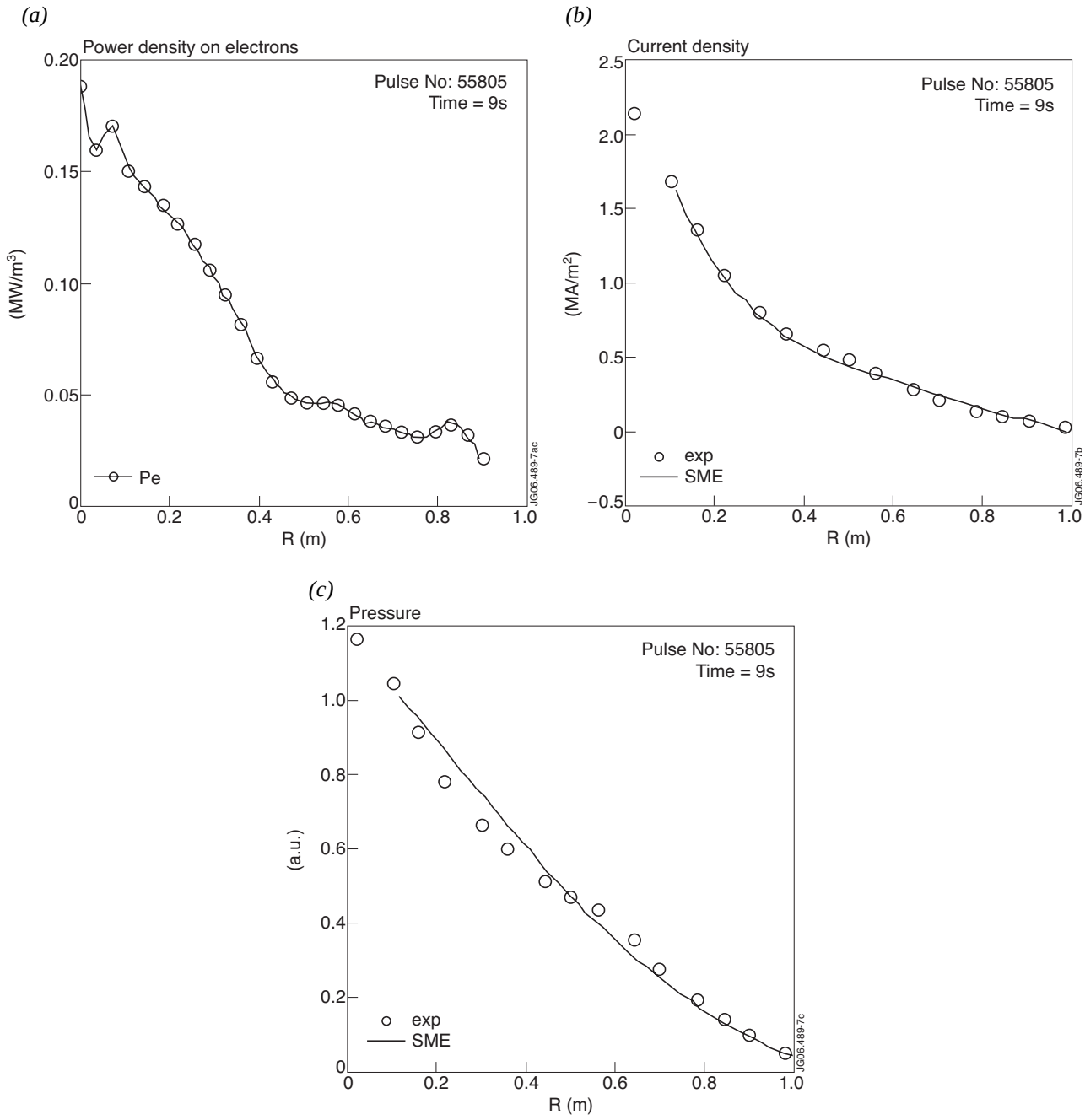

Figure 7: JET Pulse No: 55805 NBI+ICR heated L-state; (a) radial profile of the power density on electrons; radial theoretical (line) and experimental (circles) profiles of the total current density (b),(including 0.20MA of non inductive current) and of the normalized pressure (c) in the range 1<q<5.88.

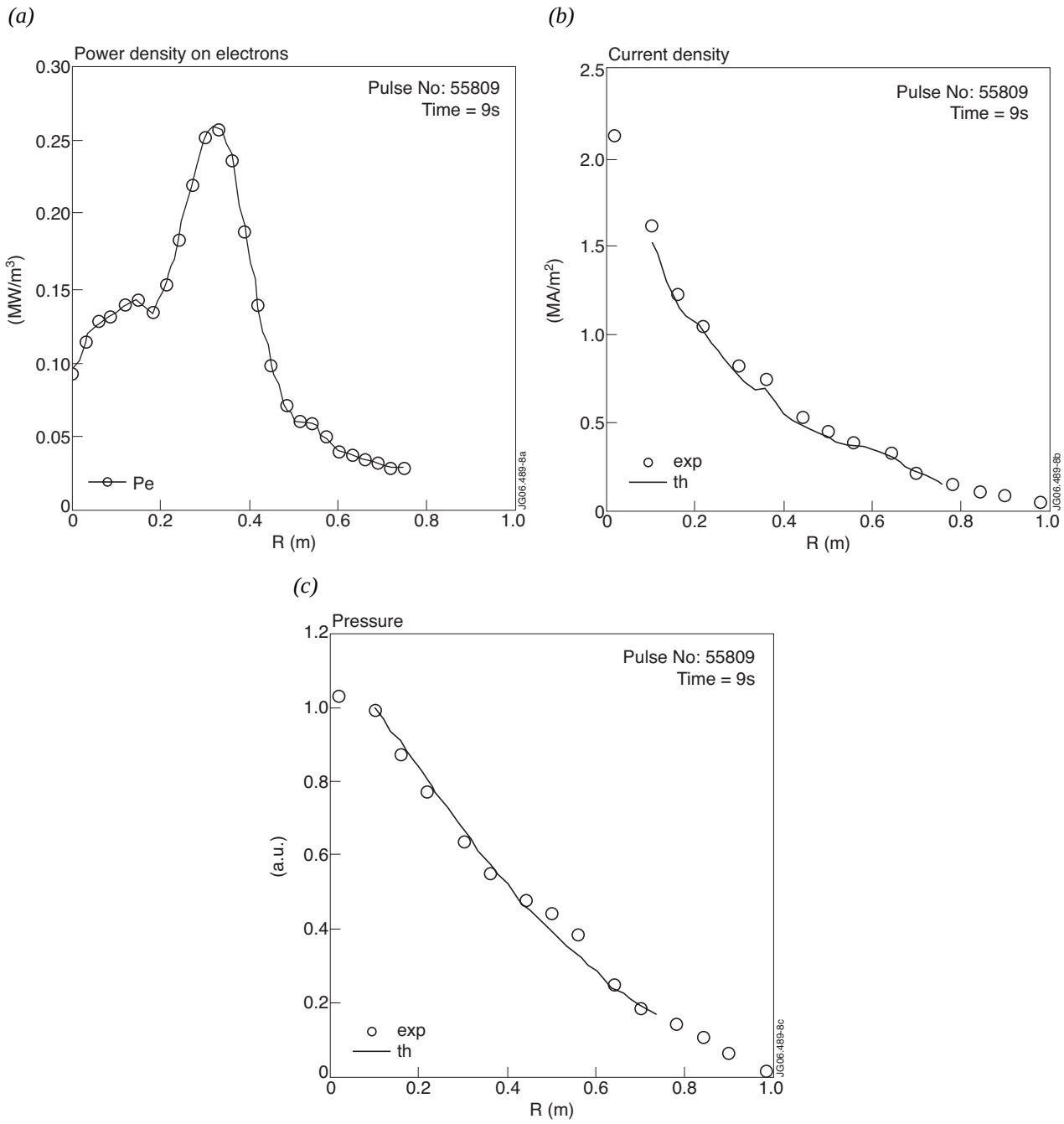

Figure 8: JET Pulse No: 55809 NBI+ICR heated L-state; (a) radial profile of the non Ohmic power density on electrons; radial theoretical (line) and experimental (circles) profiles of the total current density (b) (including 0.27MA of non inductive current) and of the normalized pressure (c) in the range 1<q<3.92.

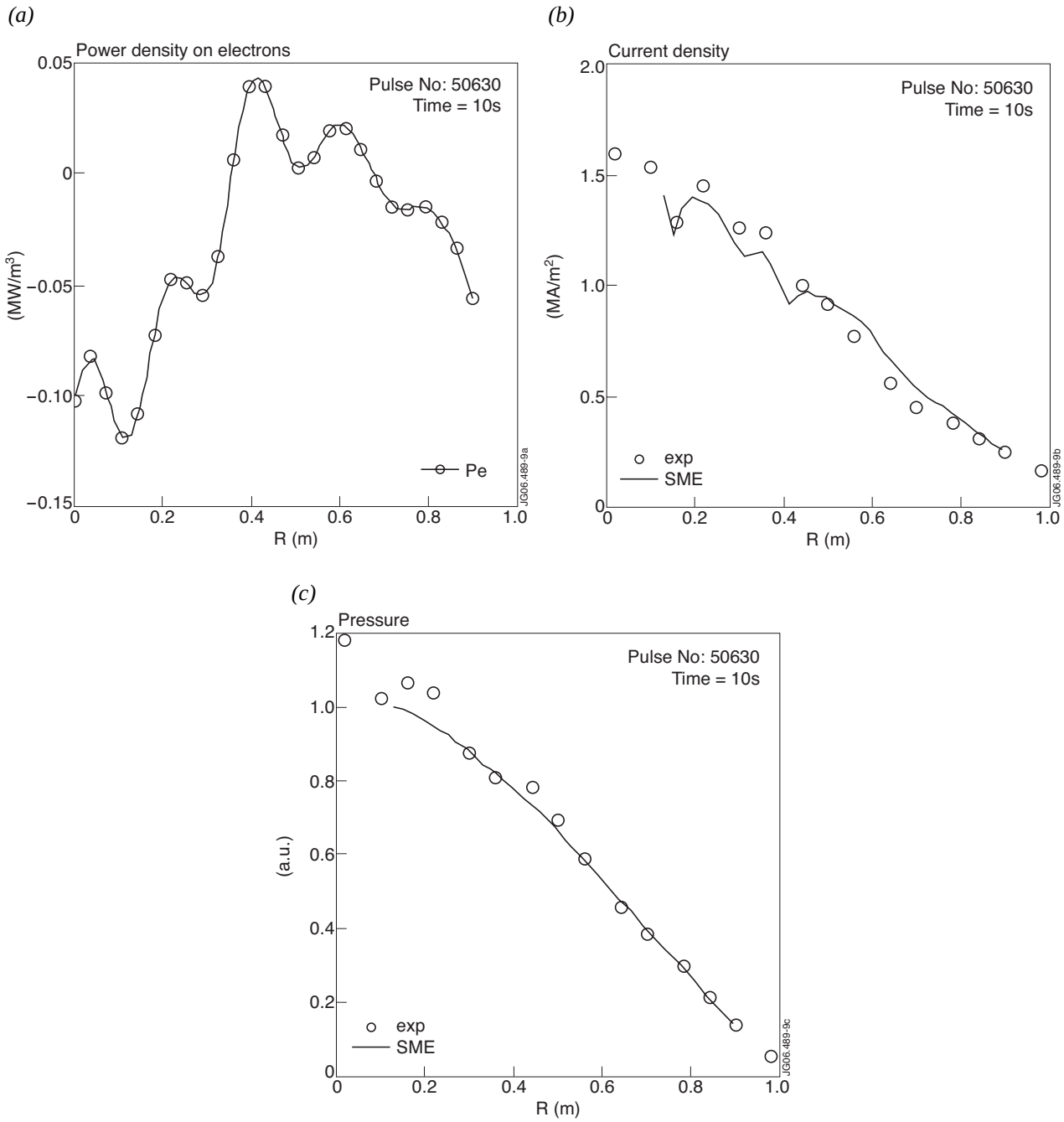

Figure 9: JET Pulse No: 50630 NBI+ICR heated H state with high density ($n(0)\cdot 10^{-20} = 0.70$); (a) radial profile of the non Ohmic power density on electrons; radial theoretical (line) and experimental (circles) profiles of the total current density (b) (including 0.22MA of non inductive current) and of the normalized pressure (c) in the range $1.03<q<2.78$.

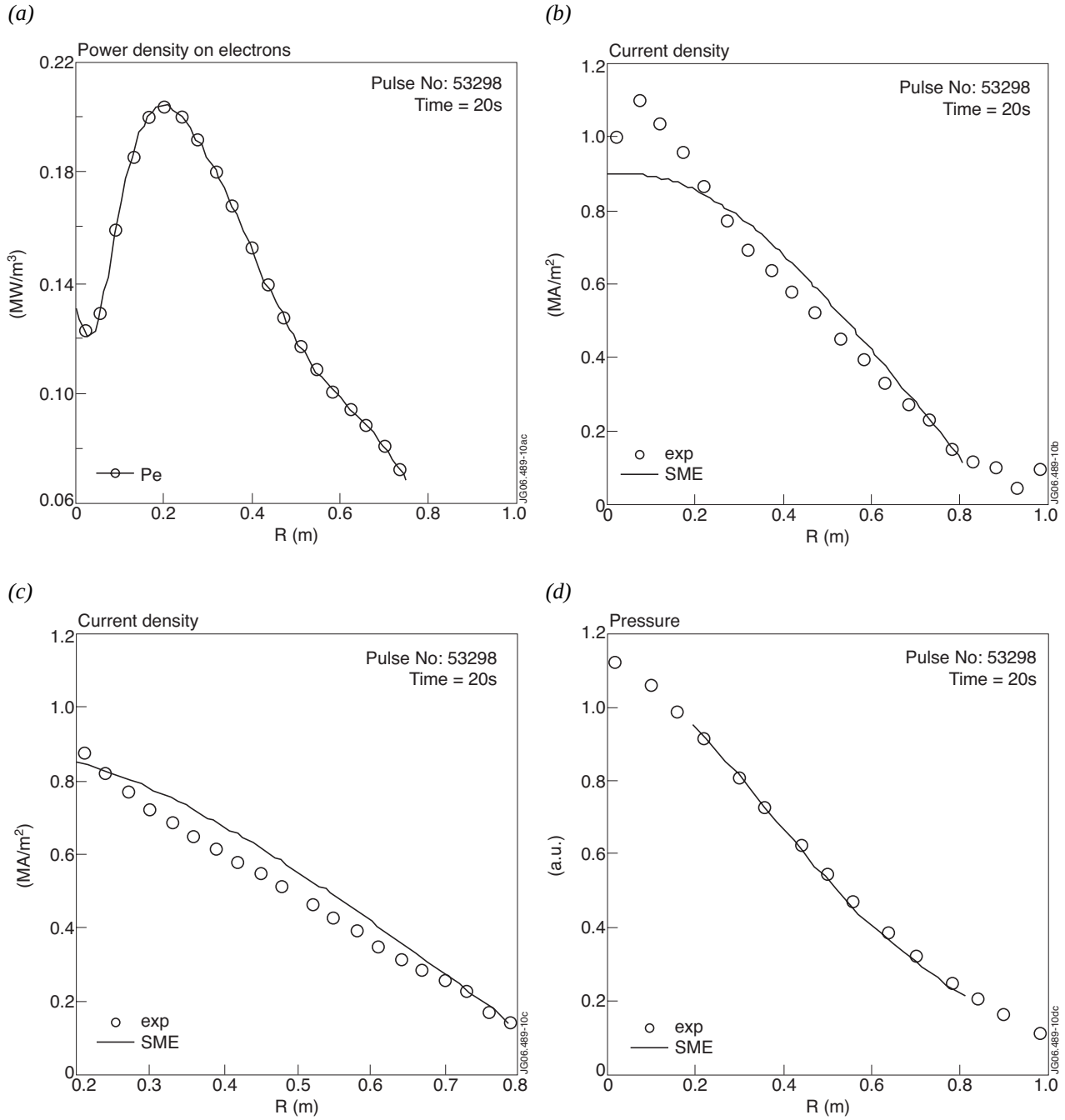

Figure 10: JET Pulse No: 53298 NBI heated H state; (a) radial profile of the non Ohmic power density on electrons; (b) solution of the SME equation with zero derivative on axis (line) and experimental profile (circles) with hole on axis ($q_{min} \approx 1.3$); theoretical (line) and experimental (circles) profiles of the current density (c) and of the normalized pressure (d) in the outside zone $1.41<q<3.22$ with $r(m)>0.20$.

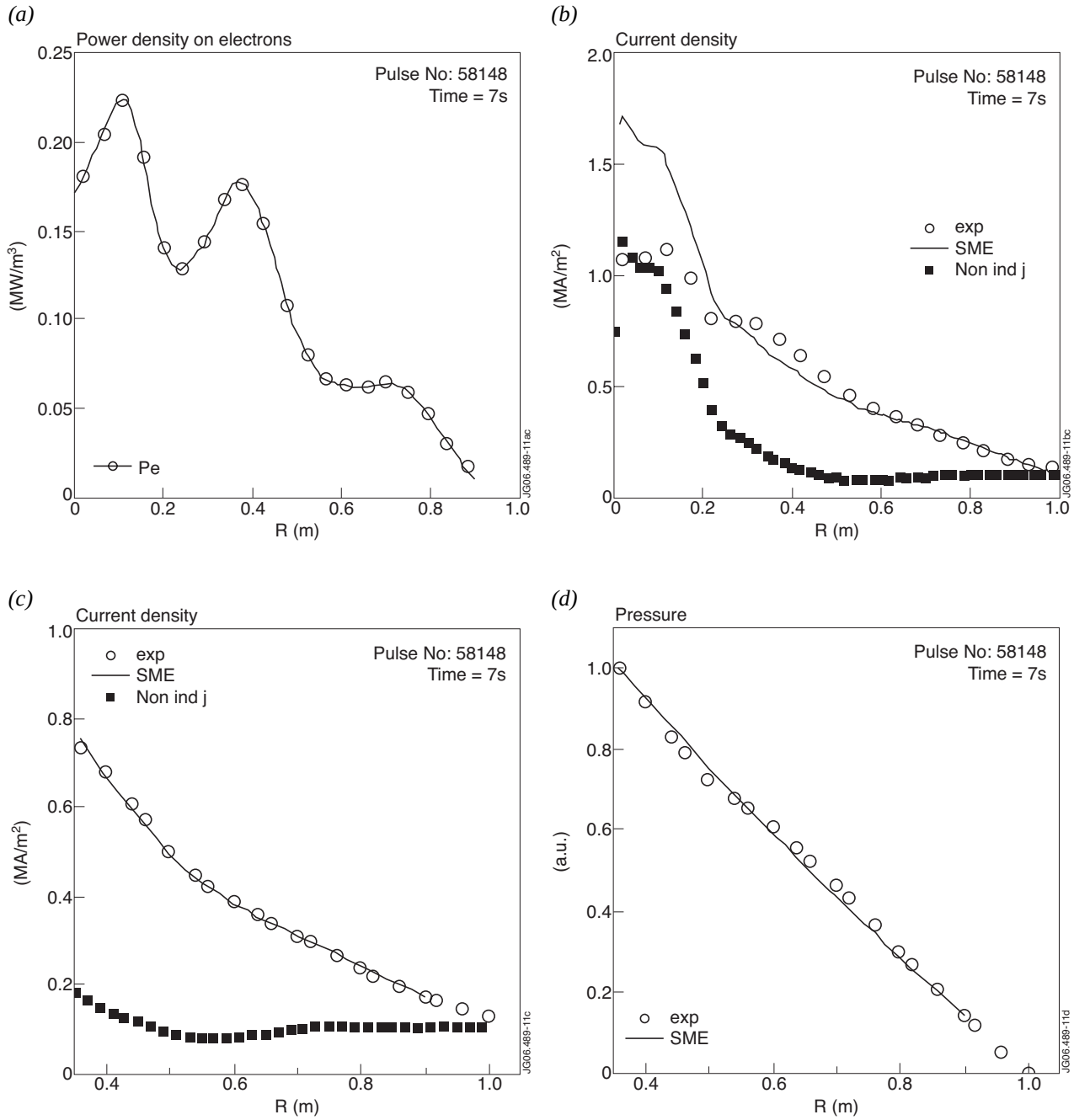

Figure 11: JET Pulse No: 58148 NBI+ICR heated H state with intense non inductive current in the central region ($q_{min} \approx 1.5$);(a) radial profile of the non Ohmic power density on electrons; (b) total theoretical (line) and experimental (circles) current density and the non inductive part (dots); (c) theoretical (line) and experimental (circles) profiles of the current density and of the non inductive part (dots) in the outside zone 2.17<q<5.36 with r(m)>0.36; (d) theoretical (line) and experimental (circles) normalized pressure in the same zone.

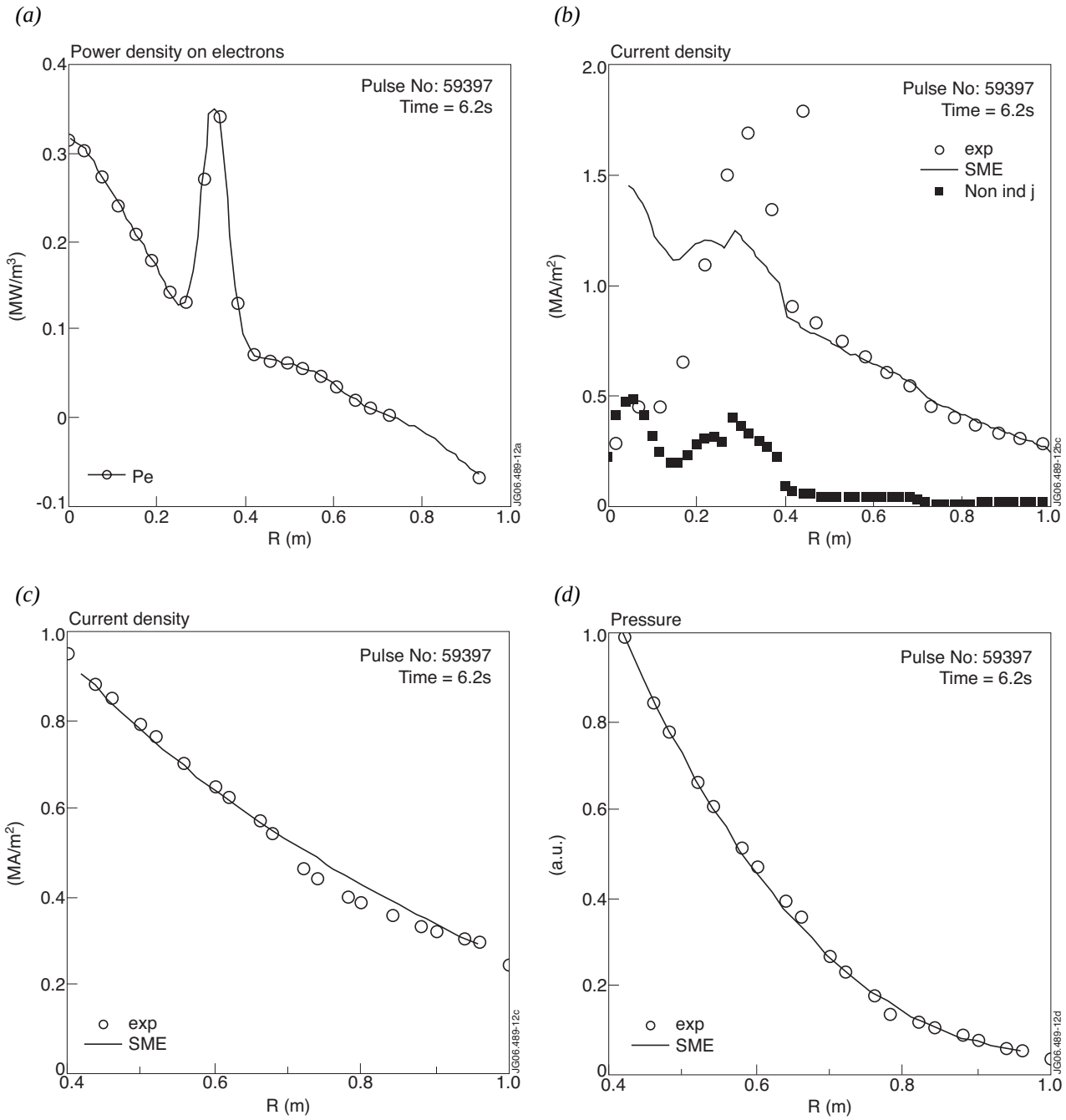

Figure 12: JET Pulse No: 59397 NBI+ICR heated with internal transport barrier($q_{min} \approx 1.6$) and 0.38MA of non inductive current. (a) radial profile of the non Ohmic power density on electrons; (b) total current density, including the non inductive part (dots), obtained from the solution of the SME equation with zero derivative on axis (line) and experimental profile (circles) with deep hole on axis. Theoretical (line) and experimental (circles) profiles of the current density (c) and of the normalized pressure (d) in the outside zone 1.71<q<4.33 with r(m)>0.42.